Journal of
Applied Remote Sensing

Soil moisture derived using two apparent thermal inertia functions over Canterbury, New Zealand

Mammatt Sohrabinia
Wolfgang Rack
Peyman Zawar-Reza

SPIE

Soil moisture derived using two apparent thermal inertia functions over Canterbury, New Zealand

Mammatt Sohrabinia,[a,c,*] Wolfgang Rack,[b] and Peyman Zawar-Reza[a]

[a]University of Canterbury, Centre for Atmospheric Research, Department of Geography, Ilam, Christchurch 8140, New Zealand

[b]University of Canterbury, Centre for Antarctic Studies and Research, Gateway Antarctica, Ilam, Christchurch 8140, New Zealand

[c]Ministry for Primary Industries, Spatial, Forestry & Land Management, 25 The Terrace (Pastoral House), Wellington 6011, New Zealand

Abstract. The near-surface soil moisture (SM) is an important property of the soil that can be studied from satellite remote sensing observations over a large spatial domain. This research provides an estimate on the accuracy of SM retrieved from satellite land surface temperature (LST) observations over the Canterbury Plains, New Zealand. The apparent thermal inertia (ATI) method with two approaches (ATI1 and ATI2) was applied to derive the near-surface SM from the moderate resolution imaging spectroradiometer (MODIS) LST product. The *in-situ* measurements of SM and rainfall data at six sites across the study area were used as reference. The analysis was conducted over two periods, a short period of four months and a longer period of three years. SM simulations by the weather research and forecasting (WRF) model were used in the analysis for the shorter period. Overall, SM based on ATI2 showed a slightly higher correlation with the *in-situ* measurements ($\bar{\rho} = 0.66$) than ATI1 ($\bar{\rho} = 0.63$). The correlation, in general, was higher for the WRF simulations ($\bar{\rho} = 0.81$). Both functions performed better during summer compared to winter, but overall, ATI2 showed lower mean errors (ME $\approx -15\,m^3 \cdot m^{-3}$ volumetric SM) compared to ATI1 (ME $\approx -20\,m^3 \cdot m^{-3}$) at most of the sites. Additionally, seasonal variations of SM were better detected by ATI2 than ATI1, and the effects of precipitation were detected on more occasions by the ATI2 function. We conclude that ATI2 function can be used to estimate the near-surface SM over a large area from the MODIS LST time series if a few representative reference stations are available. [DOI: 10.1117/1.JRS.8.083624]

Keywords: moderate resolution imaging spectroradiometer; near-surface soil moisture; rainfall; apparent thermal inertia; land cover; time series.

Paper 13470 received Nov. 22, 2013; revised manuscript received Apr. 3, 2014; accepted for publication Apr. 28, 2014; published online May 22, 2014; corrected May 23, 2014.

1 Introduction

The near-surface soil moisture (SM) affects diurnal change of surface temperature, and is a key variable in computing several parameters of the land energy and water budget.[1] Observations of spatially distributed SM are essential for a large range of hydrological, climate, and agricultural applications.[2]

Satellite observations in the visible and near-infrared (VNIR), thermal infrared (TIR), and microwave (MW) regions of the electromagnetic radiation can be used to derive the near-surface SM[3,4] with a varying depth depending on the surface type and the energy employed by the sensor. Land surface temperature (LST) is the parameter measured by TIR observations. One of the algorithms based on TIR datasets is the thermal inertia (TI) method.[5] The apparent thermal inertia (ATI), a quantification of the effect of soil TI on soil surface temperature, is

*Address all correspondence to: Mammatt Sohrabinia, E-mail: sohrabinia.m@gmail.com

solely based on remotely sensed observations.[3,4,6] ATI makes use of the difference between day and night LST as well as surface albedo information derived from VNIR observations.[7]

Methods for retrieving the near-surface SM using ATI mainly differ in their approach to estimate the diurnal cycle of LST. Ref. 8 developed a model (known as XC) to derive the real TI from the advanced very high resolution radiometer (AVHRR) day (14:37 local solar time) and night (04:44) observations and found that TI is directly proportional to ATI. To compute the real TI, the XC method required an extra parameter measured on the ground, which was the time of the maximum temperature in daytime obtained from a meteorological station. Ref. 9 developed a method based on three AVHRR LST observations per day (02:30, 7:30, and 14:30 local solar time) to retrieve TI without the need for a ground measured parameter. The same authors developed another model,[10,11] named FTA (four temperatures algorithm), using four AVHRR thermal observations (02:30, 7:30, 14:30, and 19:30) and compared their method with XC. They found that FTA is better in presenting the diurnal cycle of soil surface temperature as it uses more LST observations over a 24-h period. Ref. 6 also used two LST observations (day and night) from Meteosat, but to estimate ATI rather than TI. They approximated the topsoil saturation index from ATI and scaled it using the maximum and minimum long-term SM measurements on the ground to obtain the near-surface SM content (we will call this ATI1 function). Ref. 4 modified FTA to be applied on the moderate resolution imaging spectroradiometer (MODIS) LST observations from Terra and Aqua day and night (~1:30, 10:30, 13:30, and 22:30) overpasses (we will call it ATI2 function).

The LST product is one of many datasets derived from day and night observations of MODIS onboard Terra and Aqua satellites for more than a decade. MODIS BRDF/Albedo product is another dataset, which is useful as a necessary input for ATI calculations. As a property of land surface, SM can also be estimated based on surface moisture fluxes; therefore, coupled land atmospheric models with regional scales are also used to simulate SM across spatial extent. The weather research and forecasting (WRF) community model is a mesoscale regional model, which can be used to simulate SM over scales ranging from meters to thousands of kilometers[12] when it is coupled with one of the available land surface schemes in the model. Using numerically modeled SM in combination with a remote sensing approach can be helpful to fill the gaps in the latter due to cloud cover. It also provides the opportunity for intercomparison of the two outputs over spatial domain. This is critically important on areas where ground truth data are not available (such as rugged alpine or densely forested parts of the South Island of New Zealand).

The objective of this research, therefore, is to assess the relationship between SM derived from the MODIS LST using the ATI method, simulated by the WRF model and measured on the ground, and to compare the performance of ATI1 and ATI2 functions. The study is aimed to find out if a more detailed representation of the LST diurnal cycle in the ATI model leads to an improvement in the near-surface SM retrievals. Based on our review of the literature, there have been limited attempts previously to compare different ATI methods and to evaluate their performance in relation to rainfall.

2 Study Area

The study area covers part of the Canterbury Plains in the South Island of New Zealand (Fig. 1), approximately centered at 43° 37′ S and 172° 11′ E. Surface elevation of the study area ranges from a few meters near the coast to about 200 m above sea level (asl) near the Southern Alps in the West. The Canterbury Plain is the largest area of flat land in New Zealand dominated by agricultural and farming land use. Widespread use of irrigation is an ever increasing need in the region to sustain productivity. For the same reason, study of soil water content over a large spatial extent is a prime concern in this region. Only satellite data and modelling approaches can provide an adequate coverage of SM variability over this extensive spatial domain. To obtain consistent results, however, remotely sensed data and modeled parameters need to be validated based on ground measurements.

Measurements of SM at six sites across the study area (Fig. 1) were used as reference. The land cover (LC) types of these sites were dominantly grass mixed with trees, irrigated crops, urban developed areas, and barren/fallow land (Fig. 2 and Table 1).

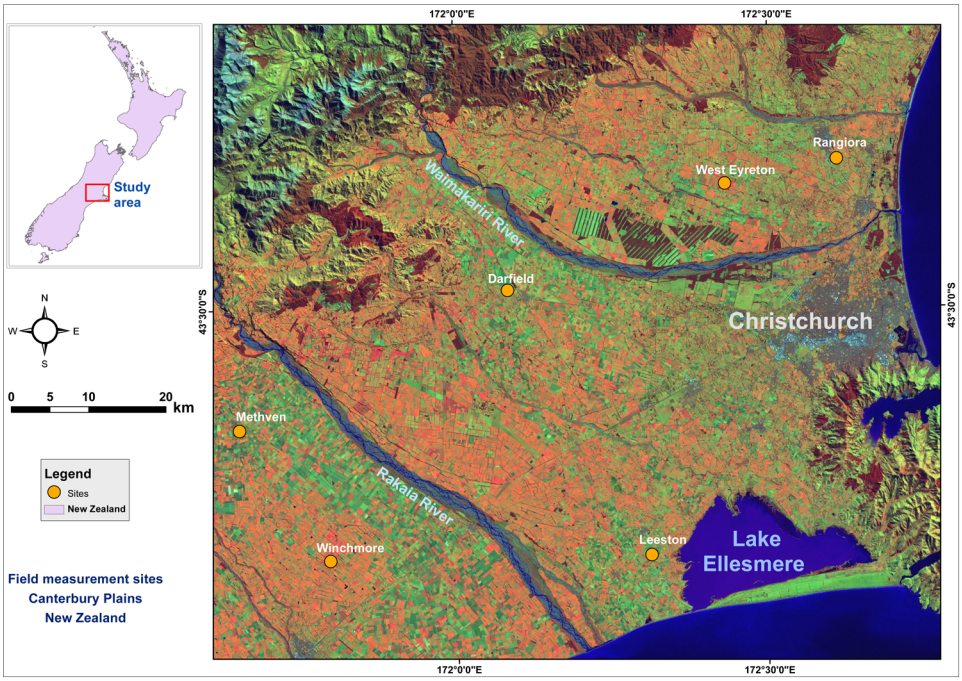

Fig. 1 Map of the study area with the *in-situ* soil moisture measurement points overlaid on a false-color (bands 4,5,2) Landsat image (TM 5, captured on 28 March 2011).

Fig. 2 Land-cover types of the *in-situ* soil moisture measurement sites at (a) Rangiora, (b) Methven, (c) Leeston, (d) Winchmore, (e) West Eyreton and (f) Darfield (imagery from Google Earth).

3 Data

Data used in this paper include the *in-situ* measurements of SM and rainfall, the remotely sensed LST and albedo products, and the WRF simulations.

3.1 *In-situ Measurements*

The *in-situ* measurements of SM (20-cm depth) over a period of three years (January 01, 2010, to December 31, 2012) recorded at six automatic stations across the study area (Fig. 1) are used in this research. These data were downloaded from the national climate database- Cliflo (http://cliflo.niwa.co.nz) of New Zealand, which is maintained by the National Institute of Water

and Atmospheric Research (NIWA, http://www.niwa.co.nz). These data were recorded with an hourly rate, but were downgraded to a daily rate to match the daily frequency of ATI SM derivations. Daily rainfall data, accumulated over a period of 24 h, were also downloaded from these stations for the same period to be used in the analysis. Additional *in-situ* measurements of the near-surface SM (2 to 5 cm depth) over five LC types were also collected in the field; however, these measurements turned out to be highly affected by solar radiation; therefore, they were not used in the analysis.

3.2 *MODIS LST Product*

This product is an operational dataset derived from MODIS thermal observations onboard Terra and Aqua satellites. These observations are collected during day and night overpasses of Terra and Aqua (approximately at 1:30, 10:30, 13:30, and 22:30) with different viewing angles. The LST product is derived from bands 31 and 32, which are observed at 10.78–11.28 μm and 11.77–12.27 μm spectral ranges, respectively. Theoretical background and technical details of the algorithms and the procedure for extraction of LST from MODIS thermal bands are beyond the scope of this paper, but can be accessed in the literature.[13–15]

3.3 *MODIS Combined BRDF/Albedo Product*

The combined albedo product (MCD43B3) is generated from a combination of MODIS-Terra and MODIS-Aqua albedo products (MOD43B3 & MYD43B3) accumulated over a 16-day period. MOD43B3 and MYD43B3 are Level 3 global products with 1-km resolution mapped into a sinusoidal grid. As a result, MCD43B3 combined albedo product is an 8-daily dataset with the same resolution and geometric specifications[16,17] as the two preceding products. This dataset contains two types of albedos: a "black-sky albedo" (BSA), which is the directional hemispherical reflectance that integrates the BRDF over the exitance hemisphere for a single irradiance direction, and a "white-sky albedo" (WSA) which is the bi-hemispherical reflectance that integrates the BRDF over all viewing and irradiance directions.[18] Data for each of the BSA and WSA categories are derived from MODIS bands 1–7. Three more integrated broadband albedos from the visible (0.3–0.7 μm), near-infrared (0.7–3.0 μm), and shortwave (0.3–5.0 μm) regions[17,19] for each of the BSA and WSA categories are also provided in this dataset. Broadband albedo is the ratio of radiant energy scattered upward and away from the surface in all directions to the downwelling irradiance incident upon the surface[18] from all directions. The actual albedo on the ground, or "blue-sky albedo" can be estimated as a sum of BSA and WSA weighted by the proportions of direct and diffuse solar radiations arriving at the ground.[19] We interpolated both BSA and WSA fields in the 8-daily combined albedo products to daily values using a linear interpolation function. In the next step, we calculated the blue-sky albedo based on the sum of the shortwave broadband BSA and WSA weighted by 0.34 and 0.66, respectively. The advantage of this approach, rather than using a constant value for albedo in ATI calculations (which was practiced by other references[8,10]), is taking the seasonal variability of the surface albedo into account.

3.4 *WRF Simulations*

Surface layer SM simulations from the WRF model for a period of four months (July 31 to December 01, 2010) were used in this paper. We used the Noah land surface model (LSM) as a land parameterization scheme.[20] Noah LSM is one of the multiple land surface schemes coupled with the WRF modeling system.[21] The initial conditions for SM simulations in the model are defined by the National Center for Environmental Prediction (NCEP) global final analysis (FNL) data with a spatial resolution of 1×1 deg ($\sim 80 \times 111$ km in our study area) and 6-h frequency.[12] The input variables from the NCEP FNL data include (but are not limited to) soil moisture/water content, soil temperature, precipitation, heat flux, humidity, surface winds, and land cover (see http://rda.ucar.edu/datasets/ds083.2). The Noah LSM only provides surface heat and moisture fluxes as lower boundary conditions to the coupled atmospheric (i.e., the WRF) model.[22] These fluxes are then transported throughout the boundary layer, and interact

with other model physics involving cloud, radiation, and precipitation processes.[22] In the Noah LSM, the green vegetation fraction (Fg) parameter, which is defined as the coverage of vegetation over an area unit or a pixel,[12] is used to differentiate moisture flux from vegetation. As a result, the WRF model coupled with the Noah LSM is able to separate soil and vegetation moisture fluxes and also accounts for precipitation effects in SM approximation. To calculate SM, a prognostic diffusion equation for the volumetric SM content is used.[23] Sensitivity of the WRF model to different land surface parameterization schemes, such as the Noah LSM, is discussed in the literature,[12,21] which includes SM simulations. Noah LSM simulates the near-surface SM in four predefined layers (with a top-down sequence of 0.05, 0.25, 0.70, and 1.5 m depth). Outputs for the top most layer (5-cm depth) were used in our analysis. The first 24 h of the simulations were discarded from the analysis as the spin-up period required by the model to reach a balanced state with the boundary conditions. Grid spacing of the simulations was set to 5 km for the first and 1 km for the second domain of the model to match the spatial resolution of the MODIS LST. The time interval of the model outputs was set to a 30-min rate for all simulations.

4 Methods

4.1 *Thermal Inertia Approach for Soil Moisture Estimation*

TI, defined as the resistance of a material to change in temperature,[24] is calculated based on the knowledge of thermal conductivity and density of the near-surface soil layer Eq. (1)

$$\mathrm{TI} = \sqrt{\Lambda \rho C}, \tag{1}$$

where TI ($\mathrm{J \cdot m^2 \cdot K^{-1} \cdot sec^{-1/2}}$) is thermal inertia of the soil, Λ ($\mathrm{W \cdot m^{-1} \cdot K^{-1}}$) is the soil thermal conductivity, ρ ($\mathrm{kg \cdot m^{-3}}$) is the soil bulk density, and C ($\mathrm{J \cdot kg^{-1} \cdot K^{-1}}$) is the soil heat capacity.[3,25,26] Water bodies have a higher TI than dry soils and rocks, and exhibit a lower diurnal temperature amplitude (DTA), therefore, when soil water content increases, DTA of the soil will decrease.[6] This property can be exploited to derive the amount of moisture content in the upper soil from remotely sensed LST. It must be noted that in our investigation area, TI is also affected by the low to medium (mainly grass) vegetation (Fig. 1). The ATI method based on two or more daily LST observations and one daily albedo data, along with a priori knowledge about the acquisition date and the geographic latitude, is used to derive the near-surface SM from remotely sensed observations Eq. (2). ATI is defined as[3,4,6,24]

$$\mathrm{ATI} = S\frac{1-\alpha_0}{\mathrm{DTA}}, \tag{2}$$

where α_0 is the broadband albedo, DTA is derived from two or more daily LST observations, and S is the solar correction factor defined as

$$S = \sin\,\vartheta\,\sin\,\varphi(1-\tan^2\vartheta\tan^2\varphi) + \cos\,\vartheta\,\cos\,\varphi\,\arccos(-\tan\,\vartheta\,\tan\,\varphi), \tag{3}$$

where ϑ is the local latitude and φ is the solar declination, which is calculated for each day of the year.[4]

If only two observations representing coolest and warmest LST values over a 24-h period are used, the DTA will be simply the difference between the diurnal warm and cool temperatures (ΔLST), defined as[6,24]

$$\mathrm{DTA_1} = \mathrm{LST_{day}} - \mathrm{LST_{night}}, \tag{4}$$

where $\mathrm{LST_{day}}$ and $\mathrm{LST_{night}}$ are daily LST observations at peak warm and cool hours, respectively. LST observations from MODIS-Aqua with approximate overpass times at 1:30 am and pm (representing $\mathrm{LST_{night}}$ and $\mathrm{LST_{day}}$) have been often used in the literature to calculate DTA.[6] MODIS-Terra observations with approximate overpass times at 10:30 am and pm (representing $\mathrm{LST_{day}}$ and $\mathrm{LST_{night}}$, respectively) were also used by others.[24]

A second method to calculate DTA is to apply four LST values from a combination of daily MODIS-Terra and MODIS-Aqua observations[4]

$$\mathrm{DTA}_2 = 2\left\{\frac{n\sum_{i=1}^{n}\cos(\omega t_i-\psi)T_i-\sum_{i=1}^{n}\cos(\omega t_i-\psi)\sum_{i=1}^{n}T_i}{n\sum_{i=1}^{n}\cos^2(\omega t_i-\psi)-\left[\sum_{i=1}^{n}\cos(\omega t_i-\psi)\right]^2}\right\}$$
$$\psi = \arctan(\xi)+\pi$$
$$\xi = \frac{(T_1-T_3)[\cos(\omega t_2)-\cos(\omega t_4)]-(T_2-T_4)[\cos(\omega t_1)-\cos(\omega t_3)]}{(T_2-T_4)[\sin(\omega t_1)-\sin(\omega t_3)]-(T_1-T_3)[\sin(\omega t_2)-\sin(\omega t_4)]}. \quad (5)$$

In Eq. (5), $n = 4$ for four MODIS daily observations, $\omega = 2\pi/(24*60*60)$ rad s^{-1} is the angular velocity of the Earth's rotation, t_i $[i = 1,\ldots,4]$ is the overpass time, T_i is the surface temperature (i.e., LST) at each overpass time, and ψ is the phase angle.

The near-surface SM can be then calculated from the ATI values for every pixel[6] after checking for possible outliers. After calculation of ATI, Ref. 6 used the minimum and maximum ATI values over each pixel over time (t) to calculate the remotely sensed topsoil saturation index ($\mathrm{SMSI_{RS}}$) using Eq. (6):

$$\mathrm{SMSI_{RS}}(t) = \frac{\mathrm{ATI}(t)-\mathrm{ATI_{min}}}{\mathrm{ATI_{max}}-\mathrm{ATI_{min}}}, \quad (6)$$

where ATI (t) is the ATI value at time t, $\mathrm{ATI_{min}}$ is the minimum, and $\mathrm{ATI_{max}}$ is the maximum ATI values in the entire time series of the pixel under analysis.

Finally, Ref. 6 derived volumetric soil moisture content (SMC) based on the $\mathrm{SMSI_{RS}}$ values

$$\mathrm{SMC}(t) = \mathrm{SMSI_{RS}}(t)\cdot(\mathrm{SM_{sat}}-\mathrm{SM_{res}})+\mathrm{SM_{res}}, \quad (7)$$

where t is time, $\mathrm{SM_{res}}$ is the residual volumetric SMC, and $\mathrm{SM_{sat}}$ is the saturation volumetric SMC. Since $\mathrm{SM_{res}}$ and $\mathrm{SM_{sat}}$ can only be determined under laboratory conditions, field measurements are unlikely to be equal to extremely high or low laboratory values.[6] For the same reason, $\mathrm{SM_{res}}$ and $\mathrm{SM_{sat}}$ in practice are substituted by the minimum ($\mathrm{SM_{min}}$) and maximum ($\mathrm{SM_{max}}$) *in-situ* measurements of SM over the entire period, respectively (Table 1).

In this paper, ATI as given in Eq. (2) was calculated with two different approaches: ATI1 using Eq. (4) and ATI2 using Eq. (5), each of which takes a different solution to estimate DTA. In the next step, Eq. (6) is used to derive $\mathrm{SMSI_{RS}}$ at each site. Finally, we scaled $\mathrm{SMSI_{RS}}$ values to the respective $\mathrm{SM_{min}}$ and $\mathrm{SM_{max}}$ measurements at each site using Eq. (7).

Table 1 Geographic coordinates of the *in-situ* soil moisture (SM) and rainfall measurement stations alongside the minimum ($\mathrm{SM_{min}}$) and maximum ($\mathrm{SM_{max}}$) measured SM at each site during the measurement period (3 years: January 2010–December 2012), and the dominant land-cover around each site.

Station	Latitude	Longitude	$\mathrm{SM_{min}}$ (%)	$\mathrm{SM_{max}}$ (%)	Land cover
Rangiora	−43.329	172.611	11	53	Mixed grass and irrigated crop
Methven	−43.640	171.652	4	60	Grass mixed with urban
Leeston	−43.789	172.312	7	59	Grass mixed with trees
Winchmore	−43.793	171.795	1	45	Grass
W.Eyreton	−43.357	172.432	11	42	Irrigated grass
Darfield	−43.480	172.084	6	59	Grass mixed with barren/fallow

4.2 *Multitemporal Time Series Analysis of Soil Moisture from Apparent Thermal Inertia Method*

The analysis was conducted in two temporal scales: short term (four months: August 01 to December 01, 2010) and long term (three years: January 01, 2010, to December 31, 2012). The first time scale was chosen to identify the effects of rainfall on ATI SM retrievals, as well as the WRF SM simulations, and to evaluate the difference in seasonal trends in comparison to the *in-situ* measurements. Also, since model simulations of SM with a 1-km spatial resolution are time consuming and memory intensive (especially when the time period is longer than a few months), the analysis involving the WRF model was conducted only for the short-term period. The long-term analysis was necessary to evaluate the quality of ATI SM retrievals in different seasons and to find out which ATI function is more able to detect seasonal variability of SM.

4.3 *Statistical Methods*

The Euclidean distance (d_E) was applied to compare the difference between the time series of SM from ATI functions with the *in-situ* measurements Eq. (8)

$$d_E(ts_1, ts_2) = \sqrt{\sum_{i=1}^{n} [ts_1(i) - ts_2(i)]^2}, \tag{8}$$

where ts_1 and ts_2 are two time series to be compared (e.g., ATI1 and *in-situ* SM series), and n is the total number of coincident time points in both series. If ts_1 has fewer points than ts_2, the extra points in ts_2 (which are not coincident with any point in ts_1) will be excluded from the analysis.

Pearson's correlation coefficient, ρ, is used to express the absolute relationship between any two parameters, without an attempt to predict the future. The values of ρ and d_E averaged over all sites ($\bar{\rho}$ and $\bar{d}_E$, respectively) are also used to express the overall results in the study area. A cross-correlation function (CCF), expressed as Eq. (9), is used to find the approximate time lag between the ATI derivations and the *in-situ* measurements.

$$\mathrm{CCF} = \frac{1}{n}\sum_{t=1}^{n-k}(x_t - \bar{x})(y_{t+k} - \bar{y})[k = 0, 1, \ldots, (n-1)], \tag{9}$$

where n is the total number of coincident observations in both series, t is time, k is lag, and $\bar{x}$ and $\bar{y}$ are the mean values of the x and y input series, respectively.[27]

5 Results

5.1 *Short-Term Series: Apparent Thermal Inertia Results Versus Simulated and In-Situ Soil Moisture*

Derived SM from the MODIS LST using the ATI method was compared with the *in-situ* and modeled SM at six test sites for a period of four months (August to November 2010). The accuracy of the WRF simulations is analyzed to find out if these simulations can be used to compensate for the gaps in ATI derivations. Comparison between the *in-situ* data collected from a singular point in space with the MODIS pixels (or the model's grid cells) was a major concern. The issue of pixel size versus point measurements, which is already dealt with in the literature,[28,29] is a well-known problem when it comes to defining the relationship between the *in-situ* and remotely sensed gridded datasets. This issue can be partly resolved through a careful selection of the measurement point closest to the pixel center over a large, flat, and homogeneous land area. Although all of our test sites were located on flat and relatively homogeneous landscape, the *in-situ* SM measurements only represented a fraction of the overlapping pixel or grid-cell from the other two (i.e., ATI and WRF SM) datasets. As a result, a certain level of variation inside each pixel was inevitable. We tried to partly overcome this issue by choosing SM measurements at a 20-cm depth, which were considerably more homogeneous (see also Ref. 6).

Table 2 Correlation coefficient (ρ) and Euclidean distance (d_E) values between daily soil moisture time series derived from the MODIS LST (using ATI1 and ATI2) and simulated by the WRF model in one hand and the *in-situ* measurements on the other over the short-term period (August to November 2010).

	ρ			d_E		
Station	ATI1	ATI2	WRF	ATI1	ATI2	WRF
Rangiora	0.75	0.69	0.78	101	69	95
Methven	0.78	0.74	0.82	98	35	75
Leeston	0.39	0.50	0.81	51	45	59
Winchmore	0.67	0.68	0.87	86	35	69
West Eyreton	0.57	0.62	0.80	72	50	70
Darfield	0.58	0.54	0.77	83	26	93

As a result, a lower agreement between point measurements and gridded data is likely when a 1:1 correlation is applied. Therefore, more emphasis in the results will be given to the temporal profiles, and the correlation coefficient (ρ) values will be given only to provide a quantitative measure of the agreement between the two variables. ρ values were calculated between derived SM (using both ATI1 and ATI2), the WRF simulations, and the *in-situ* measurements (Table 2). For most of the sites, ρ values between the WRF and the *in-situ* data have been positive and relatively higher than the ATI SM retrievals. Overall, ATI1 and ATI2 have correlated almost similarly with the *in-situ* measurements.

Although these correlations showed almost similar results, temporal profiles of ATI1 and ATI2 SM retrievals needed to be compared to find out which approach presents a closer trend to the *in-situ* measurements and the WRF simulations. Therefore, temporal profiles of SM derived from both functions, simulated by the WRF model and measured on the ground, were overlaid on daily rainfall data (Fig. 3). The WRF simulations have shown a close match with the *in-situ* measurements, and rainfall effects are detected. The declining seasonal trend in SM amount, as observed on the *in-situ* profile, is also detected by the model but is less pronounced. Since ATI1 uses only two MODIS LST observations, there were more points possible to be calculated by this function. On the other hand, ATI2 needs four MODIS LST observations per day; thus, fewer points were possible to be modeled by this function. This is the reason that at some sites ATI2 has shown a weaker correlation (Table 2). However, it appears that the ATI2 profile is closer to the *in-situ* measurements than ATI1. Additionally, the declining seasonal trend is detected by the ATI2 function but not by ATI1.

There are more points in the later part of the analyzed period both in the ATI1 and ATI2 time series. This is due to the higher number of cloudy days in winter than in later spring. On the other hand, the model simulations have shown a larger offset with the *in-situ* measurements during the later part of the analyzed period. These results show that the ATI method is more useful in a less cloudy and warm season, unlike the WRF model, which performs better in a colder and wet season of the year. However, a longer period of analysis is required to confirm this finding, which is presented in the next section.

5.2 *Long-Term Analysis: Apparent Thermal Inertia Results versus In-Situ Soil Moisture*

The two ATI calculation functions, ATI1 and ATI2, were applied to derive the near-surface SM from the MODIS LST product for a period of three years (January 01, 2010, to December 31, 2012). Unlike the short-term analysis, this section will focus only on ATI SM derivations in comparison with the *in-situ* measurements and rainfall data.

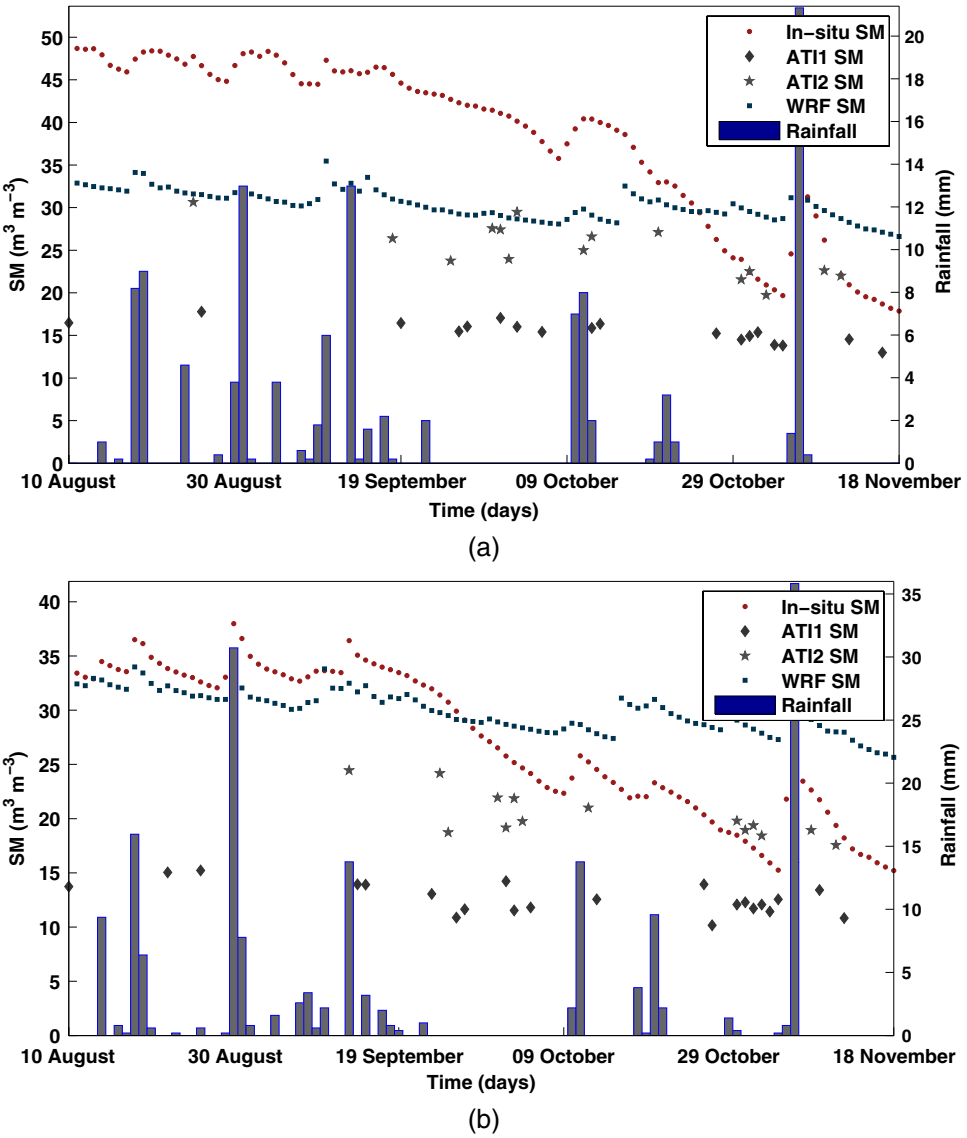

Fig. 3 Time series of soil moisture (SM) derived using ATI functions (after scaling and removal of outliers), simulated by the WRF model and recorded by the *in-situ* measurements at (a) Rangiora and (b) Winchmore sites for the short-term analysis (4 months: August to November 2010).

Table 3 Correlation coefficient (ρ), Euclidean distance (d_E) and mean error (ME) values between time-series of soil moisture derived from the MODIS LST (using ATI1 and ATI2 functions) and measured on the ground at six sites for a period of 3 years (2010–2012).

	ρ		d_E		ME (summer)		ME (winter)	
Station	ATI1	ATI2	ATI1	ATI2	ATI1	ATI2	ATI1	ATI2
Rangiora	0.77	0.76	368	213	−6	−1	−29	−21
Methven	0.67	0.78	251	119	−6	4	−21	−13
Leeston	0.42	0.51	145	82	−1	8	−18	−12
Winchmore	0.69	0.76	274	140	−7	−1	−21	−15
W. Eyreton	0.63	0.66	109	55	−2	5	−15	−10
Darfield	0.57	0.52	276	145	−5	4	−21	−14

Correlations among ATI1, ATI2, and the *in-situ* SM time series at six sites were calculated (Table 3). Because the *in-situ* measurements were made at a 20-cm depth below the surface, time lags were applied on these measurements before correlating with the derived SM time series. To discover the best time lag, the two time series (i.e, *in-situ* measurements versus ATI1 or ATI2 SM) were crosscorrelated with different time lags where every step in the lags was equal to one day. The best agreement on most sites was achieved when a time lag of one day was applied on the *in-situ* measurements. In other words, derived SM from the instantaneously observed LST data agreed best with the *in-situ* SM measured (at a 20-cm depth) one day later. The slope of change in correlations due to time lags, however, was very gradual with changes of less than 0.03 in ρ values. Thus, the actual time lag may have been slightly more or less than one day, which could be identified if data with a finer temporal resolution (such as hourly data) were available. However, retrieval of SM from the MODIS LST using the ATI method was only possible on a daily basis. Results showed that the correlations from both functions are relatively similar; however, ATI2 provided a better agreement with the *in-situ* measurements at more sites (Table 3).

As discussed before, although these correlations offer a quantitative measure of how both functions relate to the *in-situ* measurements, they do not provide information about temporal

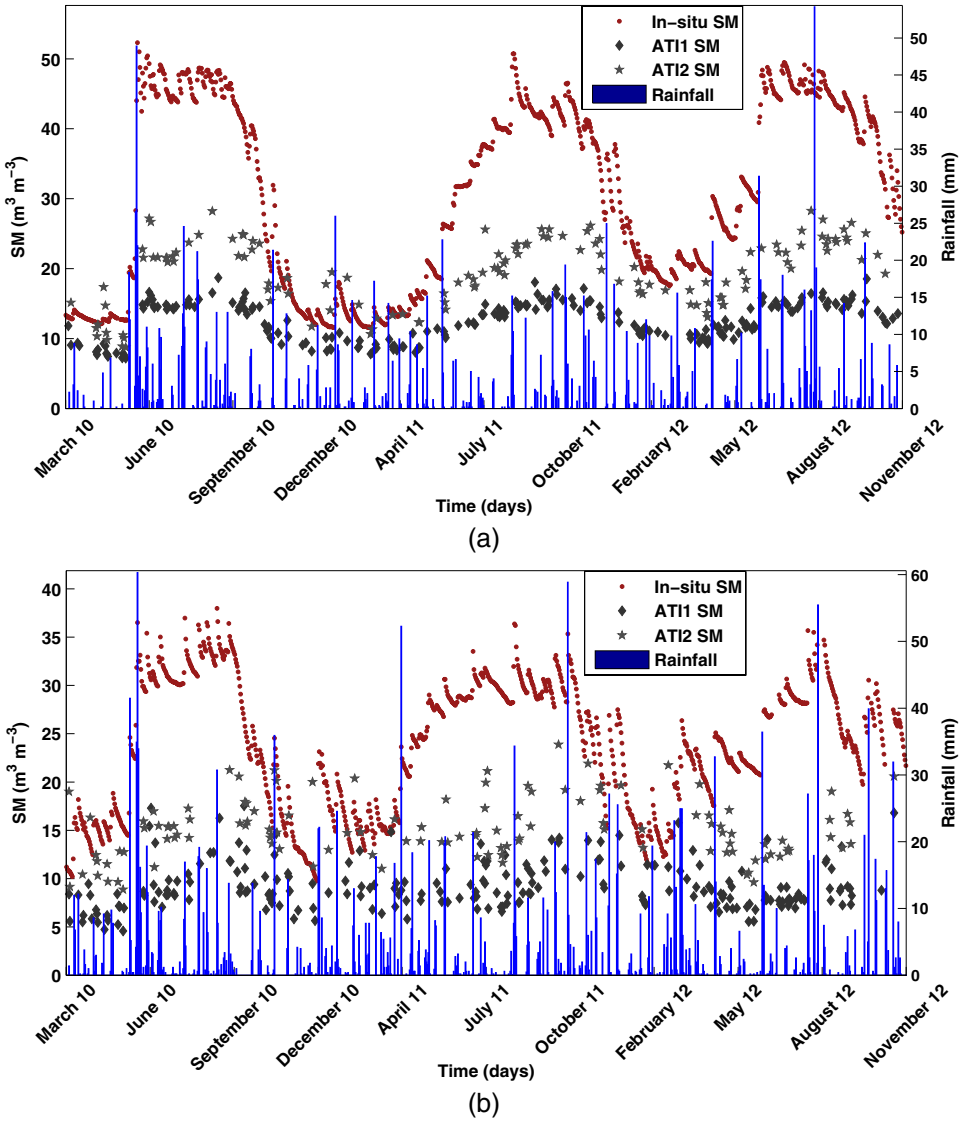

Fig. 4 Temporal profiles of ATI1 and ATI2 (after scaling and removal of outliers) compared with the *in-situ* soil moisture and overlaid on daily rainfall at (a) Rangiora and (b) Winchmore sites for a period of 3 years (2010–2012).

trends of the derived SM with respect to the ground measurements. Therefore, temporal profiles of the derived SM time series at all sites were compared with the *in-situ* measurements and overlaid on rainfall data. The results from only two sites, Rangiora and Winchmore, are shown (Fig. 4). The most striking difference between ATI1 and ATI2 SM retrievals, as shown in the long-term series (Fig. 4), is that the latter has detected the annual SM trends better than ATI1. As found in the short-term analysis, both functions have shown a better performance in a dry season. The overall bias from the *in-situ* measurements was higher during winter compared to summer. To show this quantitatively, the SM time series from both functions were separated based on winter and summer seasons and then were subtracted by the corresponding *in-situ* measurements at each site. The mean error (ME) values at each site for both seasons were then calculated (Table 3). These values showed that in summer, both functions have a small bias from the *in-situ* measurements. The ME values from the *in-situ* measurements during the wet season were considerably higher, especially in ATI1 results (Table 3). Although rainfall effects are not clearly distinguished in this temporal scale, sudden spikes in ATI2 SM are suspected to be due to rainfall. On the other hand, the ATI1 series showed a relatively smooth temporal trend with only a few sudden spikes, also suspected to be due to rainfall.

Another difference between ATI1 and ATI2 SM retrievals was the long-term offset between the two and the *in-situ* measurements. Although the ATI2 temporal trend overlaps the *in-situ* series in summer, both functions have shown a negative offset from the *in-situ* measurements for most of the three year period. To show this quantitatively, d_E was applied. The time series of SM from ATI1 showed a larger difference with the *in-situ* time series than ATI2 at all sites (Table 3). It must be mentioned, however, that these d_E values were calculated based on the absolute SM amount ($m^3 \cdot m^{-3}$) for the whole period; therefore, the one time series which had more points, tends to show more difference. As mentioned before, ATI2 had less points (due to the need for four daily LST observations) than ATI1 (which only needed two daily LST values). Therefore, the larger difference from ATI1 was partly due to more data points it its series. Since the ATI2 function uses both MODIS-Aqua and MODIS-Terra daily LST values, the DTA employed by this function contains more details. As a result, the temporal profile of SM derivations from this function is able to provide more details about SM variability in the long term. On the other hand, since four LST observations are required by ATI2, any missing LST has resulted in no SM retrieval for that day. This effect has been less severe on ATI1 as the possibility of having two cloudless LST per day is higher than four.

We also noticed that the prominent spikes due to rainfall events in the ATI series (especially ATI2) have occurred with a slight lag after the rainfall events. This was also shown in the correlations above (Table 3), where the best agreements were achieved when a time lag of one day was added to the *in-situ* SM measurements. It indicates that the changes in LST due to rainfall, as colder temperatures and smaller diurnal amplitudes, have been recorded by MODIS shortly after rainy days. Any changes in LST during the actual rain events (as a result of higher soil water content) are not available in the LST dataset due to cloud effects. As mentioned above, one way to fill these gaps in the ATI SM time series is to use the model simulations.

6 Discussion

Although satellite observations of SM based on TI are expected to capture the near-surface conditions, comparison with the *in-situ* SM measured at 2–5-cm depth turned out to be inconclusive in our investigation area. It is likely that these ground measurements have been affected by the local conditions and possibly direct solar radiation, hence, were highly variable within only a few meters' distance. This made a comparison not meaningful. Our analysis showed that SM measurements become relatively homogeneous over similar LC types in deeper soil (10 to 20-cm depth). Hence, to avoid the anomalies in the near-surface SM measurements, the authors used root-zone SM in the analysis after testing the time lag potentially required for moisture to reach a 20-cm depth in the soil.

The authors interpolated the 8-daily MODIS albedo product to daily for use in the ATI model. This approach may miss changes in surface albedo due to rainfall and cloudy conditions over the period of 8-day intervals. These changes, however, do not have a significant effect on LST-based SM derivations and can be cancelled out by the ATI model due to the following reasons. Rainfall

affects the albedo of both wet and dry soil reducing the overall reflectance and surface temperature. Since we know that ATI is based on the difference between the maximum and minimum daily LSTs (Sec. 4), it can be assumed that rainfall will have a relatively similar effect on both temperatures. LST data are also not available when there is cloud cover, hence, no SM can be retrieved in cloudy conditions (see Fig. 3).

Our results showed that the agreement between the *in-situ* measurements at some sites, such as Leeston and Darfield, and the ATI SM retrievals were relatively poor in both short-term and long-term analyses. The Leeston site was close to Lake Ellesmere. Thus, it is suspected that the MODIS LST data over this site have been affected by water. This can be partly due to a spatial mismatch between the actual LST pixel overlying this site and the neighboring pixels over the lake. However, geometric mismatching in the MODIS LST grid had been already checked by overlaying this dataset on other spatial data from the study area (such as coastal boundaries and rivers) in a GIS (Geographic Information Systems) environment (Fig. 5). Proximity to mountains or local effects (such as irrigation) can be the reason for the poor correlations from the Darfield site. Irrigation is practiced widely during the summer to keep the grass growing in the farmlands across the study area. Irrigation effects may have caused higher SM in ATI estimations at those sites for the summer season, which can reduce the overall agreement with the ground measurements. Similarly, irrigation can cause anomalies in the *in-situ* data if the measurement site is not well located. It can cause significant divergence from the normal SM trend over a localized small area, which is not necessarily captured by the satellite observations or computed by the WRF model. Since the *in-situ* measurements were acquired from an already existing online database (Sec. 3), it was not possible for the authors to make sure that the measurements were not affected by irrigation. However, a quality check of the SM measurements based on rainfall data demonstrated that there were no external anomalies in the data except for the effects of rainfall. This can be checked in Figs. 3 and 4, where the only reasons for changes in SM appear to be due to rainfall and seasonal temperature variations.

The results also showed that the WRF model has agreed well with the *in-situ* measurements. Although this analysis was only conducted in the short-term period, these high correlations indicate that the WRF model can also be relied on for a longer period. As explained in Sec. 3.4, the initial conditions for the WRF coupled with the Noah LSM are based on the NCEP reanalysis data. The reanalysis data are produced operationally every 6 h by NCEP with a 40-km spatial resolution[12] based on the upper air and surface observational data collected from the measurements in the local weather stations via the global telecommunications system (GTS). The model also combines land surface parameters, such as the surface LC and vegetation fraction[12] to produce simulations. As a result, the ability of the model to incorporate observational data in the land surface parameterization schemes can be the reason for a good agreement with the ground measurements. However, there are two main drawbacks for a modeling system as opposed to a remotely sensed approach. First, the spatial resolution of the model is limited and the

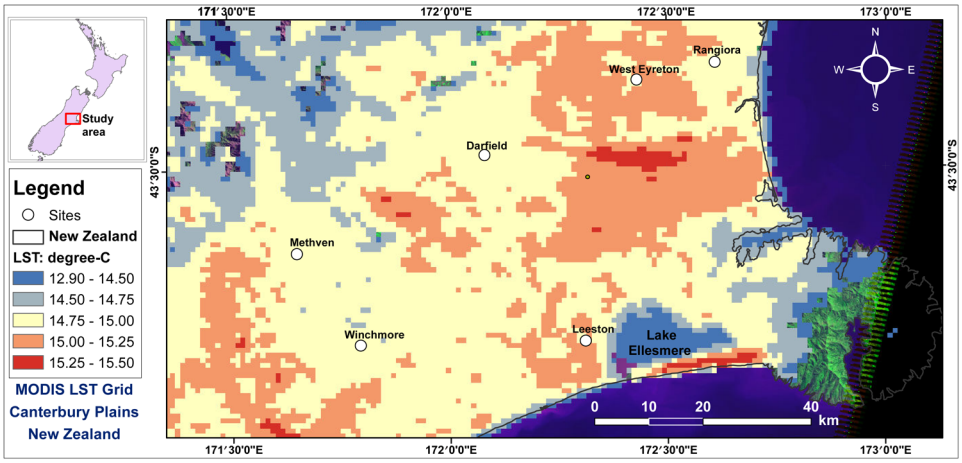

Fig. 5 Spatial matching between the MODIS LST grid and the coastal boundaries of the study area. Variations of LST over land and lake are also clear on this map.

Table 4 Summary table to compare the performance of ATI1 and ATI2 functions for soil moisture derivation from the MODIS LST observations. The mean correlation coefficient ($\bar{\rho}$) and Euclidean distance ($\bar{d}_E$) values provided in this table are averages of the results from six test-sites.

	Short term			Long term	
Parameter	ATI1	ATI2	WRF	ATI1	ATI2
$\bar{\rho}$	062	063	0 81	0.63	0.63
$\bar{d}_E$	0 82	0 43	0 77	237	0.123
$\bar{M}E$ (summer)	—	—	—	−4	0.3
$\bar{M}E$ (winter)	—	—	—	−21	−14

uncertainties increase when downscaling to a very fine resolution ($\leq$1 km) is required. The second limitation is the computational time and cost for model simulations as well as the dependence of simulations on the availability of re-analysis data, which itself depends on the availability of measurements from permanent weather stations [Sec. 3(4)]. Satellite data, on the other hand, are available nearly real-time across the globe regardless of topography or distribution of weather stations and are readily available with a predefined spatial resolution. The WRF model coupled with the Noah LSM, therefore, can be a complementary solution to fill the gaps in SM retrievals from the MODIS LST data. An intercomparison of simulated and satellite-based SM by itself also can be useful for future research on both numerical modeling and/or remotely sensed retrieval of SM over moderate vegetation (mainly grass as in our study area) in New Zealand.

Although a simple 1:1 correlation helped us to find out which function offers a higher agreement with the *in-situ* SM measurements, comparison of ATI1 and ATI2 temporal profiles enabled us to figure out which function is better able to detect seasonal trends and rainfall effects. Temporal profiles also assisted us with the interpretation of the declining seasonal trends and rainfall effects in the WRF simulations. Overall, the ATI2 retrievals showed a better agreement with the *in-situ* measurements and rainfall events than the ATI1 outputs (Table 4). This indicates that using four daily LST observations from MODIS presents a better approximation of SM than the two (a minimum and a maximum) LST used by ATI1. This is because more often LST observations enable mapping the TI of the surface and interpretation of the day and night temperature difference.[30] However, the drawback of using four daily LST observations is that more uncertainty due to the satellite ground track variations is introduced into the ATI model. Additionally, using four LST observations by ATI2 results in more missing SM retrievals as opposed to ATI1, which needs only two daily LST values.

The lower correlations at some sites (Leeston and Darfield) and the missing SM values revealed that a remotely sensed approach for SM retrieval is limited to favorable weather conditions and suitable LC types. As the results showed, the accuracy of SM retrievals deteriorate over water, dense vegetation, and rugged terrain. Sensitivity of LST to SM differs for the canopy and the soil surface beneath the plants, and is much greater for bare soil than for canopies.[31] As a result, the accuracy of the ATI algorithm diminishes over dense vegetation. The retrievals are not possible under cloudy conditions. These limitations indicate that a remotely sensed method for SM retrieval can work only in regions with favorable conditions. Such a method, therefore, is not suitable for parts of New Zealand that have dense vegetation and rugged topography. Nevertheless, an intercomparison of simulated and retrieved SM over the moderately vegetated (mainly grass) LC types, as assessed in this study, can be useful for both modeling and satellite-based studies in the future.

7 Conclusion

Soil moisture derived from remotely sensed LST, simulated by a numerical model, and measured on the ground, was analyzed in this paper. The objective of the analysis was to understand the potential of the MODIS LST dataset for soil moisture retrieval using the ATI method and to

compare the accuracy of two ATI functions based on the ground measurements. A land-atmospheric coupled model was also evaluated for potential gap filling of ATI soil moisture retrievals.

Both ATI functions showed almost similar results in the short-term (four months) period, but the overall correlation between the ATI2 time series and the *in-situ* measurements was slightly higher ($\bar{\rho} = 0.63$) than ATI1 ($\bar{\rho} = 0.62$). At some sites (such as Leeston), both functions showed relatively poor correlations. It was discussed that the poor results at those sites were due to the effects of the nearby water bodies or mountains. The WRF simulations, on the other hand, showed relatively strong correlations at all sites ($\bar{\rho} = 0.81$). The model simulations also agreed well with the *in-situ* measurements in detection of rainfall effects and the general seasonal trend. Over the long-term analysis (three years), ATI2 showed slightly higher correlation ($\bar{\rho} = 0.66$) than ATI1 ($\bar{\rho} = 0.63$). Temporal profiles of the two functions showed a considerable offset from the *in-situ* time series in the long-term analysis; however, the overall bias in ATI2 retrievals was lower ($\bar{d}_E = 126$) than ATI1 ($\bar{d}_E = 237$), partly due to the fewer points in its series. To break down this overall bias into seasons, ME values during summer and winter for all sites were calculated. Both functions showed small biases from the *in-situ* measurements in summer ($\sim 5\,\mathrm{m}^3 \cdot \mathrm{m}^{-3}$ volumetric SM), but considerably larger biases in winter with a slightly better result from ATI2 ($\bar{\mathrm{M}}\mathrm{E} = -14\,\mathrm{m}^3 \cdot \mathrm{m}^{-3}$) compared to ATI1 ($\bar{\mathrm{M}}\mathrm{E} = -14\,\mathrm{m}^3 \cdot \mathrm{m}^{-3}$). The ATI2 temporal profile was able to detect seasonal variations of SM better than ATI1. It was discussed that this is due to the more detailed DTA employed by ATI2 compared to the simple DTA of ATI1.

Results of this research indicate that the ATI2 function is more suitable for SM derivations in the study area. Since the MODIS LST product is available for more than 10 years and the mission is still being continued, long-term series of SM can be derived using the ATI2 function. Considering the good performance of the WRF model, the gaps due to cloud cover in ATI retrievals can be filled in by the model simulations.

Acknowledgments

This research was conducted under funding and support of the University of Canterbury in New Zealand. The authors would like to thank Justin Harrison for his help in the field experiment that was conducted for this research. We also acknowledge Graeme Plank from the Physics Department for providing us climate data, as well as permission for setting up our instrument in the Birdlings Flat site. Language editions and proof reading of the paper were done by Caroline Cameron-Blackgrove. We greatly appreciate very useful comments from two anonymous reviewers, which helped us in presentation and discussion of our findings. Free access to NASA's MODIS LST and MODIS BRDF/Albedo datasets is also appreciated; we used Reverb tool to download these datasets.

References

1. X. Zhang et al., "Estimation of bare surface soil moisture using geostationary satellite data," in *Proc. Geoscience and Remote Sensing Symposium, 2007. IGARSS 2007. IEEE International*, pp. 1931–1934, IEEE, Barcelona (2007).
2. M. Pause et al., "Near-surface soil moisture estimation by combining airborne L-band brightness temperature observations and imaging hyperspectral data at the field scale," *J. Appl. Remote Sens.* **6**(1), 063516 (2012), http://dx.doi.org/10.1117/1.JRS.6.063516.
3. L. Wang and J. Qu, "Satellite remote sensing applications for surface soil moisture monitoring: a review," *Front. Earth Sci. China* **3**, 237–247 (2009), http://dx.doi.org/10.1007/s11707-009-0023-7.
4. J. Vandoninck et al., "The potential of multitemporal Aqua and Terra MODIS apparent thermal inertia as a soil moisture indicator," *Int. J. Appl. Earth Obs. Geoinf.* **13**(6), 934–941 (2011), http://dx.doi.org/10.1016/j.jag.2011.07.003.
5. J. C. Price, "Thermal inertia mapping: a new view of the earth," *J. Geophys. Res.* **82**(18), 2582–2590 (1977), http://dx.doi.org/10.1029/JC082i018p02582.
6. W. W. Verstraeten et al., "Soil moisture retrieval using thermal inertia, determined with visible and thermal spaceborne data, validated for European forests," *Remote Sens. Environ.* **101**(3), 299–314 (2006), http://dx.doi.org/10.1016/j.rse.2005.12.016.

7. K. Badarinath and T. Chand, "Analysis of apparent thermal inertia over different land use / land cover types using envisat AATSR data," *J. Indian Soc. Remote Sens.* **35**, 185–191 (2007), http://dx.doi.org/10.1007/BF02990782.
8. Y. Xue and A. P. Cracknell, "Advanced thermal inertia modelling," *Int. J. Remote Sens.* **16**(3), 431–446 (1995), http://dx.doi.org/10.1080/01431169508954411.
9. J. A. Sobrino et al., "Thermal inertia mapping from NOAA-AVHRR data," *Adv. Space Res.* **22**(5), 655–667 (1998), http://dx.doi.org/10.1016/S0273-1177(97)01127-7.
10. J. A. Sobrino and M. H. El-Kharraz, "Combining afternoon and morning NOAA satellites for thermal inertia estimation: 1. Algorithm and its testing with hydrologic atmospheric pilot experiment-sahel data," *J. Geophys. Res. Atmos.* **104**(D8), 9445–9453 (1999), http://dx.doi.org/10.1029/1998JD200109.
11. J. A. Sobrino and M. H. El-Kharraz, "Combining afternoon and morning NOAA satellites for thermal inertia estimation: 2. Methodology and application," *J. Geophys. Res. Atmos.* **104**(D8), 9455–9465 (1999), http://dx.doi.org/10.1029/1998JD200108.
12. S. Hong et al., "Effects of vegetation and soil moisture on the simulated land surface processes from the coupled WRF/Noah model," *J. Geophys. Res.* **114**, D18118 (2009), http://dx.doi.org/10.1029/2008JD011249.
13. Z. Wan and J. Dozier, "A generalized split-window algorithm for retrieving land-surface temperature from space," *IEEE Trans. Geosci. Remote Sens.* **34**, 892–905 (1996), http://dx.doi.org/10.1109/36.508406.
14. Z. Wan, *MODIS Land-Surface Temperature Algorithm Theoretical Basis Document (LST ATBD)*. Institute for Computational Earth System Science University of California, Santa Barbara, California (1999).
15. Z. Wan et al., "Quality assessment and validation of the MODIS global land surface temperature," *Int. J. Remote Sens.* **25**, 261–274 (2004), http://dx.doi.org/10.1080/0143116031000116417.
16. A. H. Strahler et al., *MODIS BRDF/Albedo Product: Algorithm Theoretical Basis Document*, Boston University, University College London, Potsdam Institut fur Klimafolgenforschung, Beijing Normal University, University of Wales, Swansea (1999).
17. BU.edu, "MODIS BRDF/Albedo Product (MOD43B) User's Guide," http://www.umb.edu/spectralmass/terra_aqua_modis (18 June 2012).
18. A. H. Strahler et al., *MODIS BRDF/Albedo Product: Algorithm Theoretical Basis Document*, Boston University, University College London, Institute of Remote Sensing Application, Chinese Academy of Sciences, University of Wales, Swansea (1996).
19. J. Salomon et al., "Validation of the MODIS bidirectional reflectance distribution function and albedo retrievals using combined observations from the aqua and terra platforms," *IEEE Trans. Geosci. Remote Sens.* **44**, 1555–1565 (2006), http://dx.doi.org/10.1109/TGRS.2006.871564.
20. M. Sohrabinia, W. Rack, and P. Zawar-Reza, "Analysis of MODIS LST compared with WRF model and in-situ data over the Waimakariri River Basin, Canterbury, New Zealand," *Remote Sens.* **4**(11), 3501–3527 (2012), http://dx.doi.org/10.3390/rs4113501.
21. J. Jin, N. L. Miller, and N. Schlegel, "Sensitivity study of four land surface schemes in the WRF model," *Adv. Meteorol.* **2010**, 167436 (2010), http://dx.doi.org/10.1155/2010/167436.
22. F. Chen and J. Dudhia, "Coupling an advanced land surface-hydrology model with the Penn State-NCAR MM5 modeling system. Part II: preliminary model validation," *Mon. Weather Rev.* **129**(4), 587–604 (2001), http://dx.doi.org/10.1175/1520-0493(2001)129<0587:CAALSH>2.0.CO;2.
23. F. Chen and J. Dudhia, "Coupling an advanced land surface-hydrology model with the Penn State-NCAR MM5 modeling system. Part I: model implementation and sensitivity," *Mon. Weather Rev.* **129**(4), 569–585 (2001), http://dx.doi.org/10.1175/1520-0493(2001)129<0569:CAALSH>2.0.CO;2.
24. T.-Y. Chang et al., "Estimation of root zone soil moisture using apparent thermal inertia with MODIS imagery over a tropical catchment in Northern Thailand," *IEEE J. Sel. Topics Appl. Earth Obs. Remote Sens.* **5**, 752–761 (2012), http://dx.doi.org/10.1109/JSTARS.2012.2190588.

25. D. Pratt and C. Ellyett, "The thermal inertia approach to mapping of soil moisture and geology," *Remote Sens. Environ.* **8**(2), 151–168 (1979), http://dx.doi.org/10.1016/0034-4257(79)90014-2.
26. M. Minacapilli, M. Iovino, and F. Blanda, "High resolution remote estimation of soil surface water content by a thermal inertia approach," *J. Hydrol.* **379**(3–4), 229–238 (2009), http://dx.doi.org/10.1016/j.jhydrol.2009.09.055.
27. L. Zhang and X. Wu, "On the application of cross correlation function to subsample discrete time delay estimation," *Digit. Signal Process.* **16**(6), 682–694 (2006), http://dx.doi.org/10.1016/j.dsp.2006.08.009.
28. T. Jackson et al., "Validation of advanced microwave scanning radiometer soil moisture products," *IEEE Trans. Geosci. Remote Sens.* **48**, 4256–4272 (2010), http://dx.doi.org/10.1109/TGRS.2010.2051035.
29. J. Qin et al., "Spatial upscaling of in-situ soil moisture measurements based on MODIS-derived apparent thermal inertia," *Remote Sens. Environ.* **138**(0), 1–9 (2013), http://dx.doi.org/10.1016/j.rse.2013.07.003.
30. J. C. Price, "The potential of remotely sensed thermal infrared data to infer surface soil moisture and evaporation," *Water Resour. Res.* **16**(4), 787–795 (1980), http://dx.doi.org/10.1029/WR016i004p00787.
31. K. Mallick, B. K. Bhattacharya, and N. Patel, "Estimating volumetric surface moisture content for cropped soils using a soil wetness index based on surface temperature and NDVI," *Agricult. Forest Meteorol.* **149**(8), 1327–1342 (2009), http://dx.doi.org/10.1016/j.agrformet.2009.03.004.

Mammatt Sohrabinia received his BS degree in physical geography from the University of Tabriz in 2001, his MS degree in remote sensing and GIS from Shahid Beheshti University in 2007, and his PhD degree in environmental science from the University of Canterbury, New Zealand, in 2013. His research interests include remote sensing, GIS, and applications of spatial data and methods in environmental research. He is currently working on a project which is aimed to develop methods to identify New Zealand's native forest species based on remotely sensed data (including high-spatial resolution multispectral and LiDAR data) and GIS spatial analysis.

Wolfgang Rack received a PhD for satellite remote sensing and field studies in Antarctic glaciology in 2000. He is holding the position of a senior lecturer at Gateway Antarctica, the Centre for Antarctic Studies and Research at the University of Canterbury in Christchurch (New Zealand). His current research focus is the validation and application of satellite data related to near surface processes in snow and ice, and geophysical remote sensing applications.

Peyman Zawar-Reza received his PhD in environmental science in 2000. He is currently an associate professor in the Geography Department at the University of Canterbury. He spent four years as a postdoctoral fellow before joining the department in 2004. His research interests are mainly focused on numerical modelling of the atmosphere at small scales. Over the recent years, he has been applying his knowledge to several atmospheric phenomena, such as investigating the effect of microclimate in driving biodiversity in Antarctica.